Available online at www.sciencedirect.com
SCIENCE DIRECT
Polymer 46 (2005) 10506–10516
polymer
www.elsevier.com/locate/polymer

Epoxy-silica particulate nanocomposites: Chemical interactions, reinforcement and fracture toughness

G. Ragosta[a,*], M. Abbate[a], P. Musto[a], G. Scarinzi[a], L. Mascia[b]

[a]*Institute of Chemistry and Technology of Polymers (ICTP), National Research Council of Italy, via Campi Flegrei, 34, 80078 Pozzuoli (Na), Italy*
[b]*Institute of Polymer Technology and Materials Engineering, Loughborough University, Loughborough, Leics LE 11 3TU, UK*

Received 18 February 2005; received in revised form 5 July 2005; accepted 9 August 2005
Available online 26 August 2005

Abstract

Epoxy-silica nanocomposites were produced by dispersing silica-organosol particles in TGDDM/DDS resin mixtures. The resulting materials were investigated in terms of chemical interactions, curing behavior and mechanical and fracture properties. A reaction between epoxy groups and silanol groups present on the surface of the silica phase was detected, leading to an increased interfacial adhesion. The curing behavior of the epoxy matrix was not adversely affected by the inorganic phase. A conspicuous increase of modulus and yield strength was found by increasing the silica content. The reinforcement factors, i.e. the normalized modulus and yield strength, were found to be constant over a wide temperature range (25–180 °C). The activation volume and activation energy for yielding were found to decrease with silica content in the opposite manner, indicating an increased constraint of the structural segments involved in the yielding process caused by interfacial interactions between the silica particles and the epoxy matrix. Fracture mechanics tests showed that the addition of silica nanoparticles up to 10 wt% brings about a considerable enhancement in fracture toughness and an increase in the critical crack length for the onset of crack propagation. This enhancement in toughness is larger than that achieved until now with micro-sized particles.

Keywords: Nanocomposites; Epoxy resins; Reinforcement

1. Introduction

Particulate fillers are used in thermosetting resins primarily to reduce thermal shrinkage in the manufacture of castings or moulded products and to lower the coefficient of thermal expansion of finished products [1]. For coating applications fillers are used to increase the hardness and the abrasion resistance [2].

Functional fillers are used for specific purposes. For instance alumina trihydrate is used to impart fire retardancy, iron oxides for magnetic properties, and zinc oxide to produce materials exhibiting a non-linear resistivity.

Particulate fillers used in polymers normally have particle size in the region of 5–100 μm in diameter and are used at around 15–30 v%. The maximum amount used is limited by the resulting deterioration in processing characteristics and fracture toughness.

The effect of fillers in polymers has been widely studied over the last 50 years and particular attention has been placed on interfacial adhesion and surface treatments of the filler particles, as a means of improving mechanical properties and to minimise the formation of agglomerates during processing [3].

The importance of particle size has also been examined extensively and it has generally been found that mechanical properties improve with decreasing particle diameter of the filler [4].

Fillers with a high surface area/volume ratio (*S*/*V*) ratio have generally been found to give the best balance of mechanical properties [5,6]. The *S*/*V* ratio is normally associated with the level of particle irregularity, expressed as deviation from spherical geometry and level of surface roughness.

Work on the effects of particle size of natural zeolites filler in epoxy resins has also shown that better mechanical properties are achieved with the use of smaller particles [7].

* Corresponding author. Tel.: +39 81 8675201; fax: +39 81 8675230.
E-mail address: rago@ictp.cnr.it (G. Ragosta).

0032-3861/$ - see front matter © 2005 Elsevier Ltd. All rights reserved.
doi:10.1016/j.polymer.2005.08.028

In a study using glass beads as filler for bisphenol epoxy resins it was found that fracture toughness was primarily determined by the molecular weight of the resin, which determines the extent of shear yielding achievable around the filler particles [8]. In another study it was found that photoemission intensity increased tenfold in epoxy resins containing alumina particles as filler over the corresponding unfilled system. Fracture took place entirely through the epoxy matrix and the photoemission was highest in regions near the filler particle surface. This provides further evidence that the fracture toughness of filled epoxy resins is determined primarily by the fracture characteristics of the resin matrix, due to the high interfacial adhesion between filler and matrix.

On this basis, therefore, increasing the cross-linking density of network polymers is not an effective way of improving its structural properties, even if often this leads to an increase in strength and modulus.

In more recent years considerable emphasis has been placed on studies of nanofillers, particularly organoclays [9–13]. Because of their high *S/V* ratio nanofillers have been found to have a high reinforcing efficiency even at very low concentrations.

A reduction in T_g and an increase in both modulus and fracture toughness, has been observed in organoclay-nanocomposites based on tetraglycidyl diaminodiphenyl methane resin (TGDDM), cured with diamino diphenyl sulphone (DDS). This was attributed to interactions between the hydroxyl groups of the exfoliating agent used for the treatment of the organoclay and the resin components [14].

Epoxy-silica nanocomposites have also been produced by the sol–gel method. In such systems the filler was produced either separately or in situ within the matrix [15–20].

Epoxy resins containing in situ generated TiO_2 nanoparticles have also been prepared and beneficial effects on mechanical properties, such as wear resistance have been reported [21,22].

The use of nanofillers in network polymers constitute a more effective way of improving the overall mechanical properties of network polymers over direct modifications of their molecular composition.

In this study the preparation of a new nanocomposite system based on TGDDM/DDS resin and an isopropanol emulsion of silica nanoparticles is reported. It is demonstrated that stable and homogeneous dispersions of the inorganic nanospheres can be readily achieved by this approach. The reinforcing efficiency of the silica filler in TGDDM/DDS resin mixtures is examined and correlated with the chemical interactions occurring at the interface. The mechanical and fracture properties have been examined in a wide temperature range to assess the temperature dependence of the reinforcement factors and to elucidate the deformation mechanisms.

2. Experimental

2.1. Materials

The epoxy resin used was a commercial grade of tetraglycidyl 4-4′-diaminodiphenyl-methane (TGDDM) supplied by Ciba–Geigy. The hardener was 4,4′-diamino-diphenyl sulphone (DDS), obtained from Aldrich. The silica used for reinforcement was obtained from Clairant as a 30 wt% silica dispersion in isopropanol (trade name Highlink OG 502-30). It contains silica spherical particles with diameter in the region of 10–15 nm.

2.2. Sample preparation and chemical analysis of reaction products

2.2.1. Mixing and curing the resin mixture

The epoxy resin was placed in a two-neck 100 ml round bottom glass flask. The silica was added to the flask, drop wise under mechanical stirring (300 rpm) at 60 °C. The mixture was kept under mechanical stirring (700 rpm) for 20 min at 70 °C. Vacuum was applied and the temperature was gradually increased to 120 °C under magnetic stirring. Upon complete solvent elimination a clear solution was obtained. The temperature was raised to 140 °C and the hardener was added under vigorous mechanical stirring (700 rpm). After complete dissolution, the mixture was degassed under vacuum and poured in a glass mould preheated at 140 °C and treated with Lubrolene E6 releasing agent. Finally the mixture was cured at 140 °C for 16 h and post-cured at 200 °C for 4 h. With this protocol formulations ranging from 0 to 15 wt% were prepared. It was found that the highest concentration of silica nanofiller that could be added to the resin mixture without the formation of agglomerates was in the region of 10 wt%. This was determined from visual inspections to reveal the development of haziness or opacity.

The silica phase dispersed in the TGDDM monomer prior to curing was isolated and spectroscopically analyzed. To this end, the TGDDM/silica mixture was extracted in a solvent (chloroform or acetone), which selectively dissolves the epoxy monomer while precipitating the inorganic phase. The precipitate was recovered by filtration, repeatedly washed with the same solvent, dried under vacuum at 80 °C over night, and the FT-IR spectrum of the powder was taken with the KBr pellet technique.

2.2.2. Infrared analysis

Mid FT-IR spectra were recorded on powder samples dispersed in dry KBr, using a Perkin–Elmer System 2000 spectrometer equipped with a Ge/KBr beam-splitter and a wide-band DTGS detector. For the FT-NIR range, the spectra were recorded in the transmission mode on 1.30 mm thick samples, using the same spectrometer with a quartz beam-splitter. The scanned wavenumber range was 8000–4000 cm^{-1} and 32 scans were co-added for each

measurement to improve the signal-to-noise ratio. The isothermal kinetic measurements were carried out in a Specac 20100 temperature chamber modified in-house, which was fitted in the sample compartment of the spectrometer for the in situ collection of spectral data. The curing process was carried out at 140 °C for 20 h, followed by post-curing at 200 °C for 2.5 h. Both processes were conducted under a continuous flux of N_2 (60 cm^3 min^{-1}).

The FT-NIR spectra were used to estimate quantitatively the conversion, α, of the reactive groups relative to their initial concentration, defined as:

$$\alpha = \frac{C_0 - C_t}{C_0} = 1 - \frac{C_t}{C_0} \tag{1}$$

where C represents the concentration of reactive groups, and the subscripts 0 and t denote, respectively, the reaction times zero and t.

According to the Beer–Lambert relationship:

$$\alpha = 1 - \frac{A_t}{A_0} \tag{2}$$

where A represents the absorbance of the analytical peak. For the data presented herein the sample thickness does not change during cure, making thickness correction unnecessary. To evaluate the epoxy groups conversion the peak at 6058 cm^{-1} was preferred over that at 4521 cm^{-1}, since the latter is complicated by the interference of a primary amine group contribution occurring at about the same frequency [29]. To eliminate the overlapping profile due to the ν_{CH} overtones, difference spectroscopy was employed, according to the method described in detail in Ref. [29]. The conversion of primary amine groups was monitored by considering the peak at 5068 cm^{-1} [29,30].

2.3. Physical characterization of cured samples

2.3.1. Morphological examinations

The morphology of the samples was examined on fractured specimens by scanning electron microscopy (SEM). The apparatus used was a Philips SEM mod. XL20 and the fracture surfaces were coated with a gold–palladium layer by vacuum sputtering.

2.3.2. Dynamic–mechanical measurements

Dynamic mechanical tests were carried out using a Pyris Diamond DMA apparatus from Perkin–Elmer. The geometry of deformation was the single-cantilever bending mode. The tests were performed in the scanning temperature mode, in the range from −110 to 350 °C, at a heating rate of 3 K/min and with an oscillating frequency of 1.0 Hz.

2.3.3. Mechanical tests

Mechanical tests were performed using a universal testing machine (Instron model 4505), equipped with a temperature control chamber.

Values for the Young's modulus were obtained from the tangent of the force/deflection curve using 3-point bending tests, (ASTM D790 method), using rectangular specimens, 60.0×6.0×4.0 mm, and a span/width ratio of 8:1. The measurements were carried out at a cross-head speed of 1 mm/min, at temperatures varying from ambient temperature to 180 °C.

The yield strength was measured in compression on specimens, 60.0×6.0×4.0 mm, loaded along the length. The tests were carried out at different cross-head speeds and in the same temperature range employed for modulus measurements. Due to the absence of a definite maximum in the load/deformation curves the yield strength was estimated as the stress corresponding to the 5% offset strain from the elastic strain.

Fracture mechanics tests were carried out according to the ASTM D5045-99 standard method. A multiple crack length procedure was used in which single edge notch (SEN) specimens, 60.0×6.0×4.0 mm, with notch length varying from 1.5 to 4.5 mm, extended by 0.2 mm by a razor blade fixed to a micrometer apparatus, were fractured in a three point bending mode at room temperature. At least three samples for each notch length were used. The final length of the notch was measured using an optical microscope after fracturing the specimens.

The critical stress intensity factor, K_c, was calculated according to the following equation:

$$K_c = Y\sigma\sqrt{a} \tag{3}$$

where σ is the stress calculated as the outer skin stress for a rectangular beam in 3-point bending, Y is the compliance calibration factor obtained from tables quoted in the literature [23] and a is the notch length.

The critical strain energy release rate, G_c, was estimated through the equation:

$$G_c = \frac{U}{BW\phi} \tag{4}$$

where U is the energy at fracture initiation, B and W are the thickness and the width of the specimen, respectively, and ϕ is a correction factor that takes into account the rate of change of compliance (C) with crack length.

$$\phi = C\left[\frac{dC}{d(a/W)}\right]^{-1} \tag{5}$$

The values of ϕ were obtained from the tables reported in the literature [24].

3. Results and discussion

3.1. Infrared spectroscopy

In order to investigate the possible interactions between the silica particles and the surrounding epoxy matrix, FT-IR

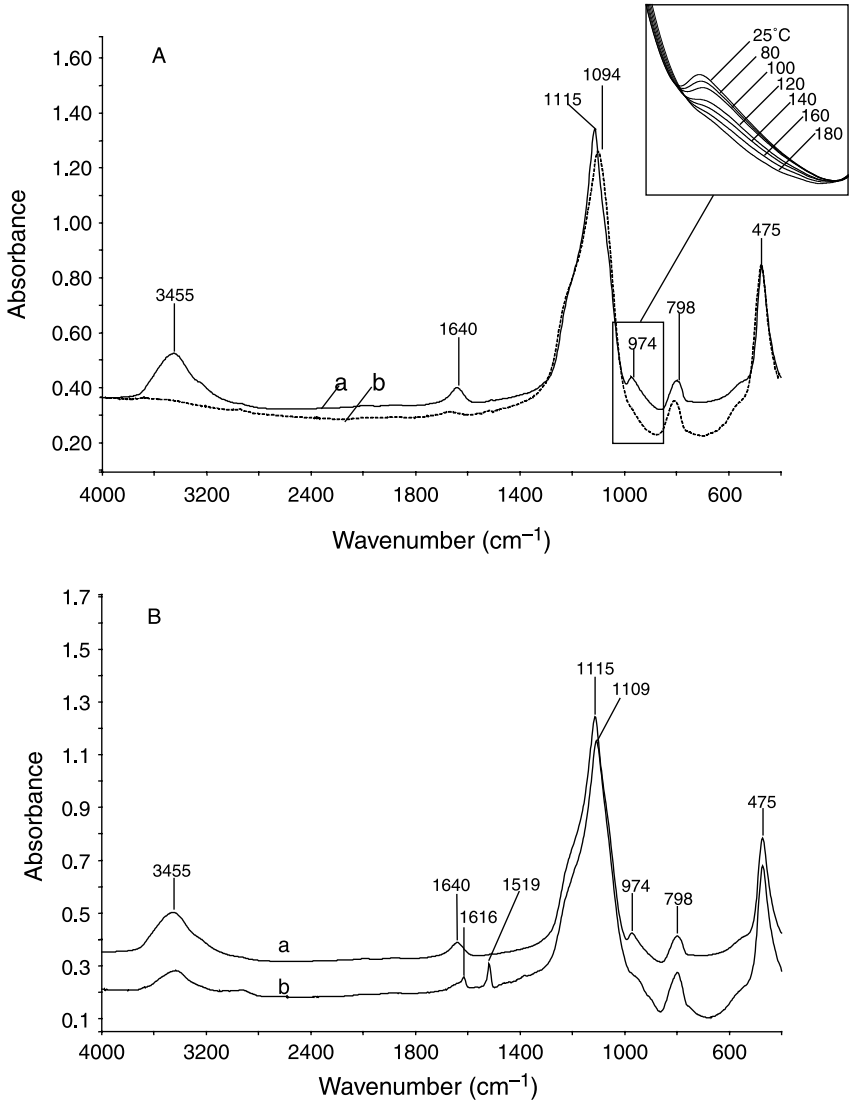

Fig. 1. (A) FT-IR spectra of the silica nanoparticles isolated from the isopropanol emulsion. Trace a, as prepared powder; trace b, the same powder thermally treated for 1 h at temperatures as indicated in the inset. The inset highlights the region 1010–850 cm^{-1} for the thermally treated sample. (B) FT-IR spectrum of the silica phase recovered from the TGDDM/silica admixture by selective precipitation (trace a). The spectrum of the starting inorganic phase is reported as trace b to facilitate the comparison.

spectroscopy measurements in the mid infrared (4000–400 cm^{-1}) were performed. Fig. 1(A) displays the transmission spectrum of the silica nanoparticles isolated from the isopropanol emulsion by solvent evaporation (trace a) and the spectrum of the same sample after 1 h annealing at 180 °C (trace b). Spectrum a is characteristic of a partially condensed silica glass, with a main absorption centered at 1115 cm^{-1}. According to recent studies, the latter band is a complex profile constituted by four main components centered at about 1220, 1160, 1090 and 1045 cm^{-1}, the exact position being dependent on condensation temperature and time [25,26]. The doublet at 1090–1045 arises from the asymmetric stretching mode of the Si–O–Si group while the two components at 1290 and 1160 cm^{-1} are likely related to the splitting of the above mode into a well separated transverse-optical/longitudinal-optical (TO–LO) pair [27,28]. The overall shape of this band is very sensitive to the molecular structure of the silica network and evolves appreciably upon thermal condensation of the glass (compare traces a and b).

The two broad bands located at 3455 and 1640 cm^{-1} originate, respectively, from the stretching and bending modes of water absorbed into the silica network, which is eliminated at high temperature. The 798 cm^{-1} peak is to be attributed to the symmetric Si–O–Si stretching vibration, while the peak at 460 cm^{-1} has been assigned to the Si–O–Si bending mode and its position has been shown to be influenced by the equilibrium bond angle [25,26]. Of particular interest in the present context is the absorption at 974 cm^{-1}, due to stretching mode of the Si–O bond in silanol groups (Si–OH) [26]. Its occurrence is indicative of incomplete condensation, with the presence of a

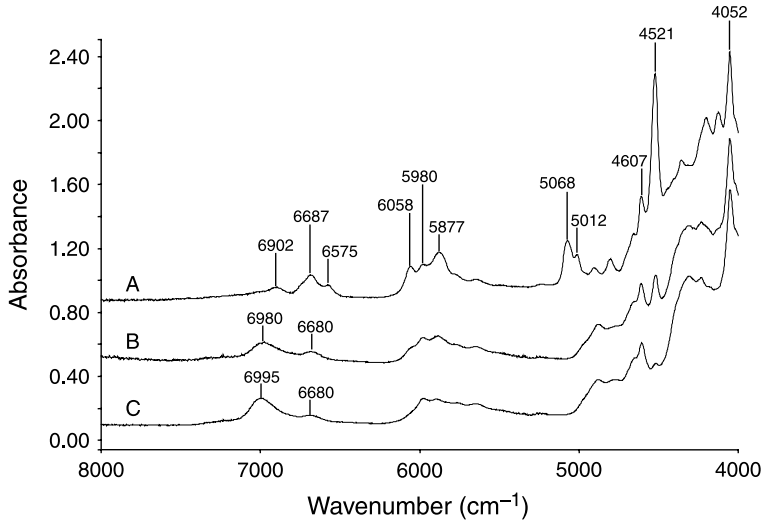

Fig. 2. FT-NIR transmission spectra in the wavenumber range 8000–4000 cm^{-1}. Trace A, TGDDM/DDS based nanocomposite with 7.0% silica before curing; trace B, above mixture after curing at 140 °C for 20 h; trace C: above mixture after post-curing at 200 °C for 2.5 h.

conspicuous amount of hydroxyl groups on the surface of the silica nanoparticles. The residual silanol groups can be further reacted by thermal treatments as demonstrated by the inset of Fig. 1(A), showing the spectra of the neat silica phase treated for 1 h at the temperatures indicated. The condensation proceeds gradually in the range 80–180 °C and can be considered complete only at 180 °C. From the above it can be concluded that the silica phase is reactive and, through its hydroxyl groups, it is capable of forming molecular interactions with proton acceptor moieties.

The homogeneous dispersion of the silica nanoparticles into the uncured TGDDM resin is achieved by mixing the components at room temperature, followed by heat treatment of the admixture at 120 °C for 1 h, for solvent elimination and degassing. After the above treatment, and prior to the hardener addition and the curing of the admixture, the silica phase was recovered by selective solvent precipitation (Section 2) and analysed by FT-IR spectroscopy. The spectrum clearly evidences the decrease of the silanol band at 975 cm^{-1} with respect to the reference spectrum (compare traces a and b of Fig. 1(B)). A semi-quantitative comparison suggests that the intensity decrease of the above band is larger than that observed for the spectrum of the pure silica phase thermally treated in the same conditions. Furthermore, two peaks are evident at 1616 and 1519 cm^{-1}, which persist, with unaltered intensity, after repeated washing cycles. These correspond to the strongest peaks of the TGDDM monomer (aromatic ring deformation modes) and indicate the presence of epoxy monomers permanently bound to the silica particles. The reaction between TGDDM and silica likely involves the epoxy and the silanol groups and is consistent with the observed decrease of the 975 cm^{-1} band. It is believed that this reaction can proceed further during the addition of the aromatic diamine hardener and the subsequent, high temperature curing steps. A definitive evidence of this hypothesis cannot be obtained at present since the presence of DDS and, even more so, the cross-linking of the system, prevent the selective dissolution of the organic components and the recovery of the silica phase.

To investigate the effect of the inorganic phase on the curing behavior of the TGDDM/DDS system, isothermal kinetic measurements were performed by means of time-resolved near infrared (NIR) spectroscopy.

The transmission FT-NIR spectra of the uncured TGDDM/DDS nanocomposite containing 7.0 wt% silica (trace A) and the spectra of the same admixture after curing at 140 °C and post-curing at 200 °C (traces B and C, respectively) are reported in Fig. 2. The overall appearance of the spectra is essentially equivalent to that of the pure TGDDM/DDS resin, since the NIR spectrum is dominated by the organic components. The two characteristic peaks of the epoxy groups were identified at 6058 and 4521 cm^{-1} [29–34]. The intensity of both absorptions decreased considerably after the curing step and disappeared almost completely after post-curing. The final conversion of epoxy groups was estimated to be in the region of 95% [29]. A partially resolved doublet at 5068–5012 cm^{-1} was attributed to a combination of stretching (ν_{s,NH_2}, ν_{as,NH_2}) and bending (δ_{NH_2}) modes of the primary amine hardener [32,33]. This feature completely disappeared after the 140 °C curing step, indicating that primary amine groups have already reacted to full conversion.

A broad band located at 6680 cm^{-1} was assigned to the first overtone of the ν_{NH} mode of the secondary amine [29,32,33]. Its intensity decreased in the spectrum of the sample after post-curing but did not vanish. This indicates that unreacted secondary amine groups are still present, even after post-curing. Finally, a band appearing at 6902 cm^{-1} in the spectrum of the unreacted resin mixture was identified and attributed to the first ν_{OH} overtone. This band was found to increases in intensity and to shift towards higher

frequencies with progressing of curing reactions as a consequence of the increasing concentration of O–H groups and the formation of a non-complex and extended H-bonding network among the latter groups.

In Fig. 3 are compared the absolute conversion ($C_0 - C_t$, expressed in mol kg^{-1}) of epoxy groups and primary amine groups, for the reaction of the nanocomposite with 7.0 wt% of silica at 140 °C. These data were derived from the α values estimated spectroscopically (Section 2), multiplying them by the relative C_0 values (i.e. $(C_0 - C_t) = C_0\alpha$).

It is seen that the two curves are coincident up to the essentially complete depletion of primary amine, indicating that, as long as the primary amine is present in the system, the sole reaction is the addition of epoxy and primary amine groups, with no side reactions taking place. Once the primary amine is completely consumed, however, the system is still reactive, as demonstrated by the ongoing conversion of epoxy groups. In these conditions the reaction of epoxy groups with secondary amine and hydroxyls constitute the main steps of the mechanism.

The above mechanistic features are characteristic of the TGDDM/DDS system [29–33], so that the kinetic analysis evidences that the cross-linking mechanism is not altered in any way by the presence of the inorganic phase, even when the silica content is quite large. This conclusion is substantiated by comparing the kinetic profiles of the epoxy groups for the 7.0 wt% nanocomposite and the unmodified resin. The curves of the relative conversion [$\alpha(t) = (C_0 - C_t)/C_0$] versus time for the two systems are essentially coincident during both the 140 °C curing step (Fig. 4(A)) and the 200 °C post-curing process (Fig. 4(B)). This result highlights the important fact that, in the present system the modifier does not adversely affects the curing rate and the reactants conversion, contrary to what is generally found for two phase systems such as TGDDM modified with an elastomeric or thermoplastic components for toughness enhancement [34,35].

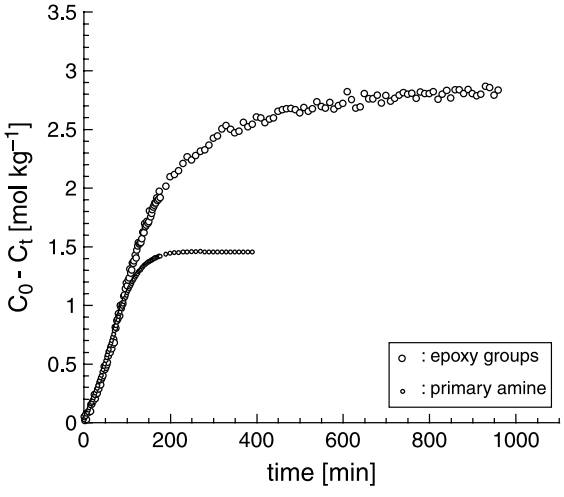

Fig. 3. Absolute conversion of epoxy and primary amine groups for the curing reaction of a nanocomposite at 140 °C.

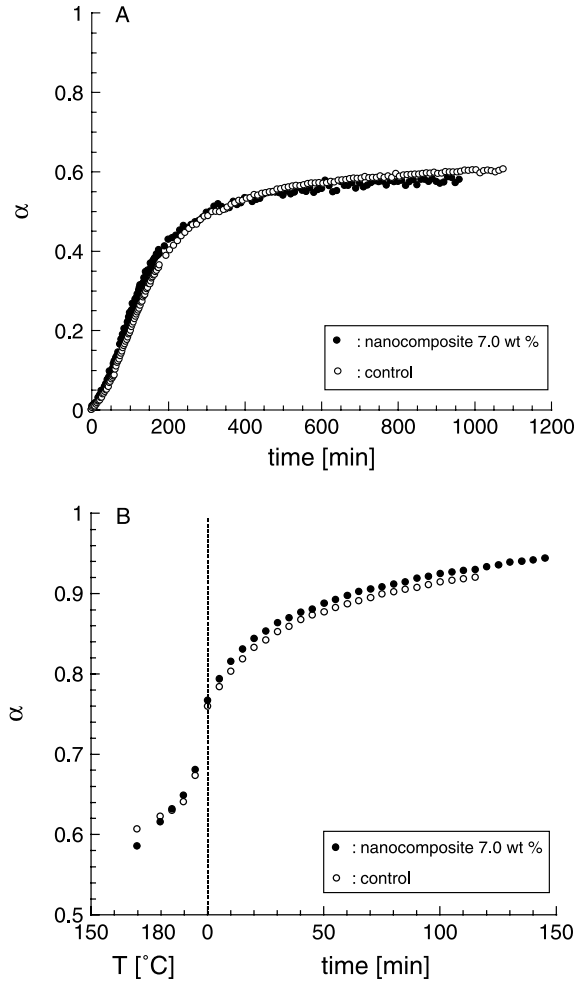

Fig. 4. (A) Relative conversion, α, of epoxy groups as a function of time for the curing reaction at 140 °C of a nanocomposite and the control resin. (B) Relative conversion, α, of epoxy groups as a function of temperature and time for the post-curing reaction of the 7.0 wt% nanocomposite and the control resin. The first section of the plot refers to the non-isothermal heating step for reaching the post-curing temperature from 140 °C (heating rate 10°/min). In this case the conversion is reported as a function of temperature. The second section is relative to the isothermal process at 200 °C.

3.2. Dynamic–mechanical analysis

Fig. 5 shows the dynamic–mechanical spectra expressed in terms of storage modulus (Fig. 5(A)) and loss modulus (Fig. 5(B)), for the pure epoxy resin (curve a) and for nanocomposites containing 5 and 10 wt% of silica (curves b and c). All samples exhibit well-defined α and β relaxation peaks at −90 and 240 °C, respectively, and a diffused ω relaxation between 30 and 80 °C. The presence of the silica nanofiller decreases the T_α value (glass transition) of about 7 °C but has no effect on the position of the β peak. The height of the both peaks, however, is decreased to an appreciable extent with the addition of the filler. The height of the ω relaxation curve is also lower for the nanocomposites but the effect is less pronounced than for the α and β relaxations.

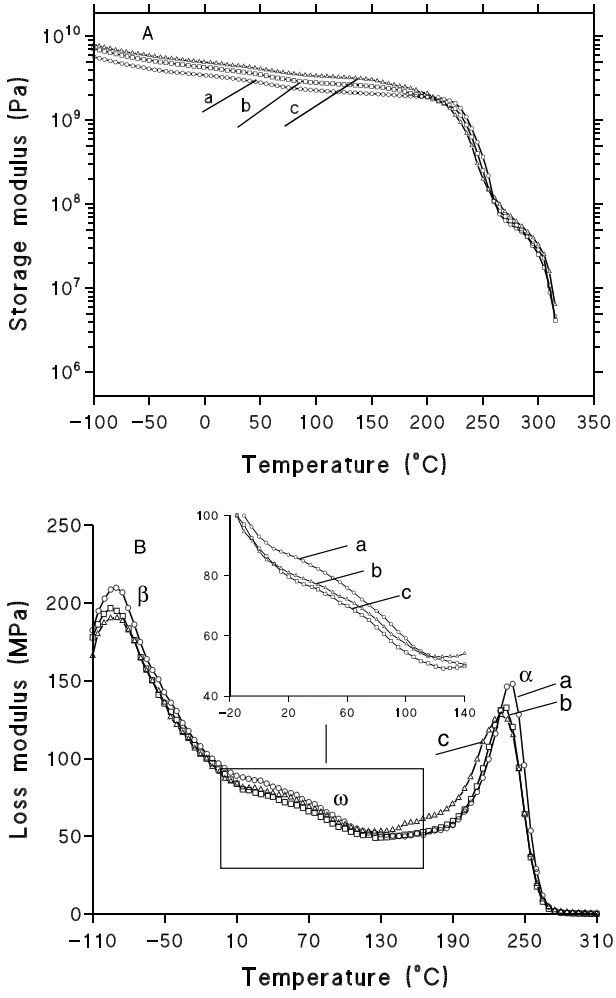

Fig. 5. Storage modulus (A) and loss modulus (B) as a function of temperature: (a) pure epoxy resin; (b) nanocomposite with 5 wt% of silica; (c) nanocomposite with 10 wt% silica.

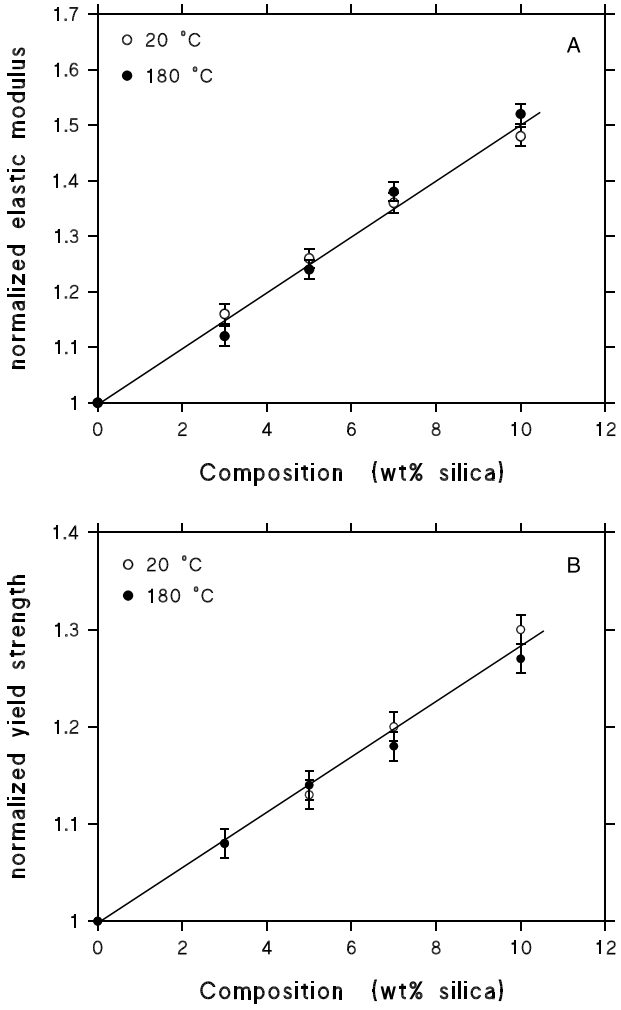

Fig. 6. Normalized elastic modulus (A) and normalized yield strength (B) at 20 and 180 °C as a function of the silica content.

The slight decrease in the T_g could be ascribed to the presence of a limited amount of unreacted epoxy resin (less than 5%), that can have some plasticization effect, while the reduction of the height of the relaxation processes can be related to the non-dissipative nature of the filler, which reduces the viscolelastic response of the composite. This also implies that the interfacial losses are very small and that the matrix/filler interfacial bonding is accordingly good. This increased interfacial adhesion leads to an overall increase in the elastic modulus, likely higher than that obtained when the interfacial losses are more pronounced.

3.3. Modulus and yield strength

In Fig. 6 are shown the data, at ambient temperature and at 180 °C, for both the normalized modulus (Fig. 6(A)) and yield strength (Fig. 6(B)) calculated as the ratio of the values for the nanocomposite to the value for the pure epoxy matrix, referred to as reinforcement factors. These show that both reinforcement factors are constant over this temperature range, reaching a value of about 1.5 for the normalized modulus and about 1.3 for the normalized yield strength, for a silica content of 10 wt%.

The higher temperature was chosen on the basis that it represents the maximum service temperature for which these systems can be used, normally as matrices for carbon fibre composites.

The effect of strain rate on yield strength was analysed by the application of Eyring's theory for the motions structural entities in a material under the influence of external stresses. For the case of deformations by yielding Eyring's theory leads to the following relationship [36,37]:

$$\frac{\sigma_y}{T} = \frac{E^*}{V^*T} + \frac{R}{V^*} \ln \frac{\dot{\varepsilon}}{A} \tag{6}$$

where E^* and V^* are the activation energy and the activation volume, respectively, R is the gas constant and A is a materials constant.

According to Eyring's equation plots of σ_y/T versus $\log \dot{\varepsilon}$ give a set of parallel lines for measurements carried out at

different temperatures. This is shown in Fig. 7 for the pure epoxy resin (Fig. 7(a)) and the nanocomposites with 5 and 10 wt% of silica (Fig. 7(b) and (c), respectively).

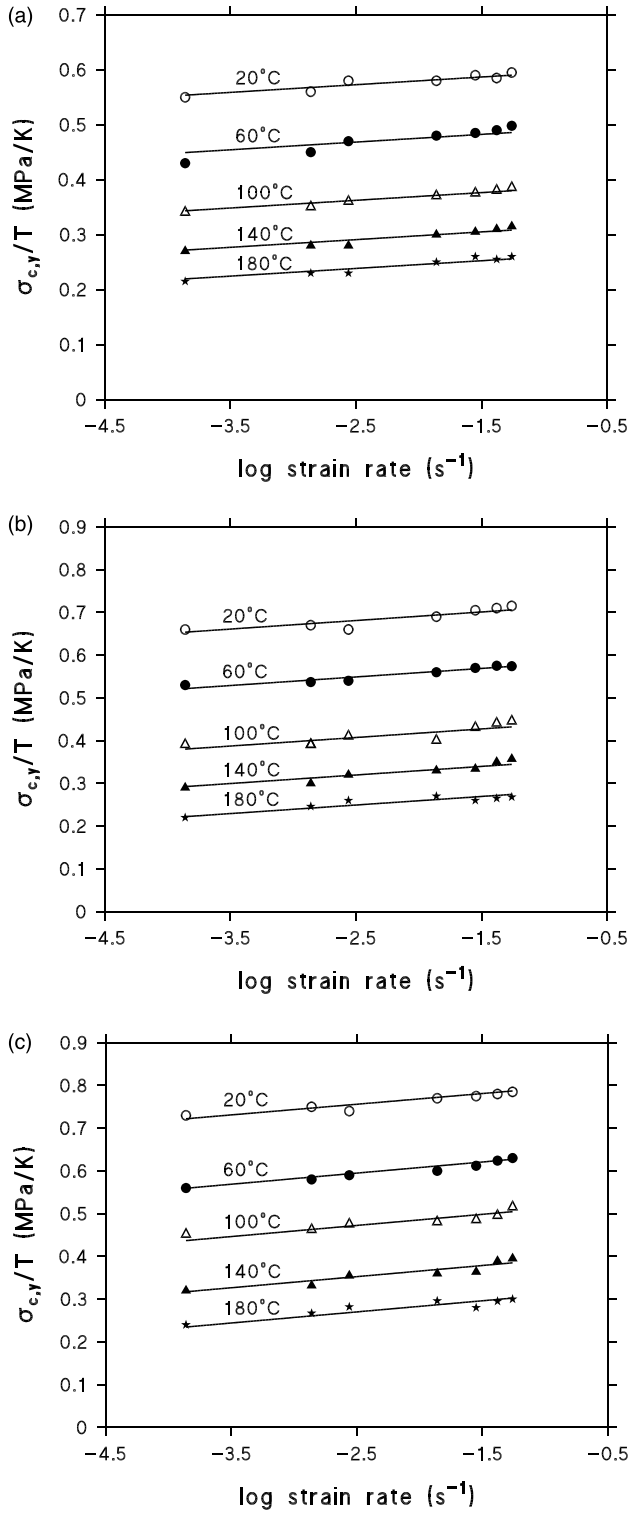

Fig. 7. Eyring plots, i.e. $\sigma_{c,y}/T$ versus log $\dot{\varepsilon}$ for (a) pure epoxy resin; (b) nanocomposite with 5 wt% of silica; (c) nanocomposite with 10 wt% silica.

Table 1
Activation energy (E^*) and activation volume (V^*) for nanocopmposites and the control resin

Sample	Activation energy (kJ/mol)	Activation volume (nm^3)
Pure epoxy resin	210	2.3
Nanocomposite with 5.0 wt% silica	301	1.6
Nanocomposite with 10 wt% silica	357	1.2

From the slope and intercept of the resulting straight lines, V^* and E^* were calculated and their values are reported in Table 1.

The correlation coefficients for the calculated values over the range of strain rates and temperatures used are higher than 0.97 in all cases. The E^* and V^* values for the pure epoxy resin compare well with those found by other authors for a series of bisphenol-A-cured DGEBA resins [38–40].

The data in Table 1 show that the activation volume, V^*, decreases with increasing silica content, while an opposite trend is observed for the activation energy, E^*.

This behaviour can be explained from considerations of the length scale of the segmental motions of the epoxy network involved in the yielding process. According to the Eyring's theory, yielding is manifest in the form of stress-activated jumps of 'flow units', which correspond to movements of network segments of the macromolecular chains.

Accordingly, the reduction in activation volume for the nanocomposite implies that a lower number of chains segments are involved in the yield process as the silica content increases. This has to result from the increased constraints on the structural segments involved in the yielding process, which are brought about by the significant interfacial interactions between the silica particles and the epoxy network. At the same time these restrictions on chain

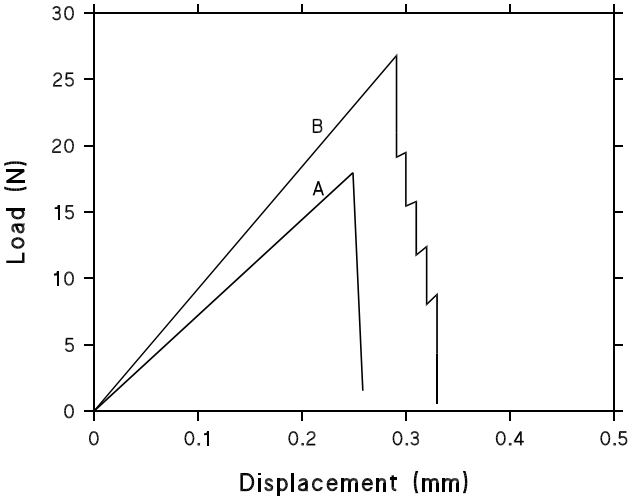

Fig. 8. Load-displacement curves: (A) pure epoxy resin; (B) nanocomposite with 10 wt% silica.

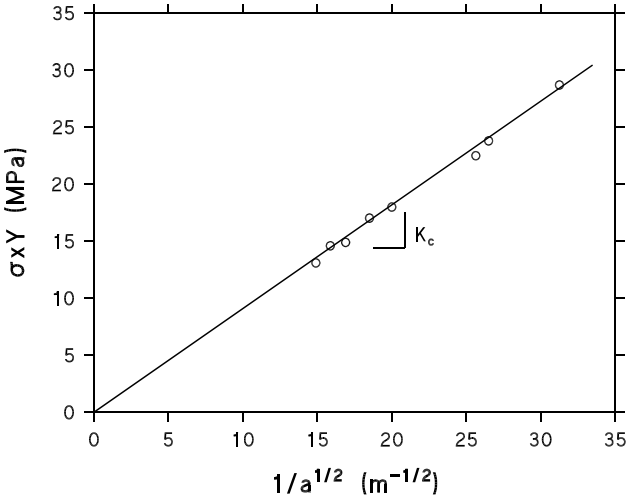

Fig. 9. Typical plot of stress to fracture against square root of reciprocal crack length for the neat epoxy resin.

mobility cause the energy barrier for yielding to increase, resulting in higher activation energy values.

A linear extrapolation of the activation energy and activation volume with increasing silica content, suggests that the activation process for yielding could be suppressed altogether at relatively low concentrations, possibly in the region of 25–30 wt%.

This implies that, under these conditions, yielding can no longer take place via segmental motions in the direction of the applied stress, but some other mechanism would have to operate. Since no other mechanism can be envisaged for highly crosslinked systems, such as TGDDM/DDS networks, at these levels of silica content failure would have to take place in a brittle fashion even under compression loading conditions.

It is worthy noting that the deformational behaviour at large strains, as experienced in flexural and compression tests, is quite different from that outlined earlier with respect to the relaxation processes in dynamic mechanical tests, where the effects of the silica filler was seen to be rather small in comparison.

3.4. Fracture behaviour and morphological examinations

Fracture of SEN specimens for the pure epoxy resin and respective nanocomposites occurred always in a brittle fashion (Fig. 8). For the case of the pure epoxy resin the load increased linearly with mid-span deflection up to the value where the crack began to propagate in a catastrophic fashion, as evidenced by the sudden drop in the recorded load (Fig. 8(A)).

In tests on nanocomposites when such loading conditions for crack propagation were reached, a series of crack stopping steps could be identified (Fig. 8(B)) indicating that the crack propagated intermittently in a stick–slip fashion. It was noted that the maximum load leading to fracture was also higher when the silica content is increased.

From the load-displacement curves the critical stress intensity factor (K_c) was evaluated by plotting the stress at fracture against $1/a^{1/2}$. On the grounds of Eq. (3) a straight line should be achieved with K_c as the slope. An example of K_c determination is shown in Fig. 9 for the neat epoxy resin. An analogous procedure was used to estimate the critical strain energy release rate (G_c). According to the Eq. (4), plots of the energy at fracture as a function of $BW\phi$ give strength lines with G_c as slopes. The values of K_c and G_c so determined are reported in Fig. 10 as functions of the silica content. This plot shows that both K_c and G_c increase significantly with the addition of low amounts of silica. In terms of G_c, the addition of 10 wt% of silica raises the fracture energy of the epoxy matrix by a factor of about four, whereas the increase in K_c is twofold. This level of enhancement is larger than it has been achieved hitherto with micron-sized particles [41–43].

In Fig. 11 are shown the micrographs taken near the crack tip for both the control epoxy resin and for nanocomposites containing 5 and 10 wt% silica. No silica

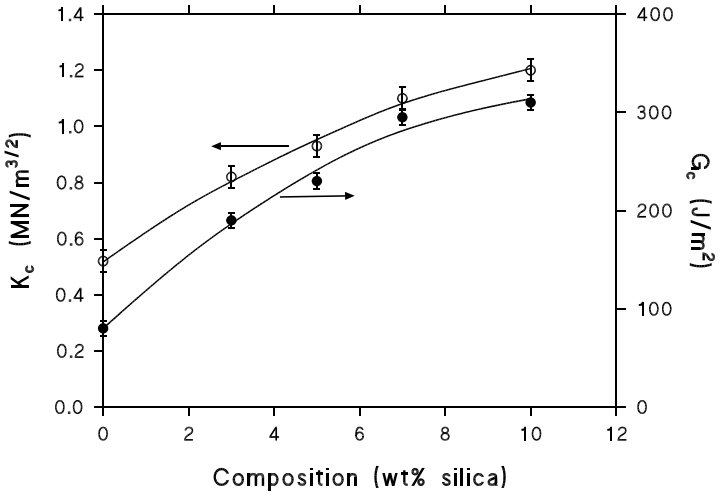

Fig. 10. Variation of the critical stress intensity factor, K_c, and of the critical strain energy release rate, G_c, as a function of silica content.

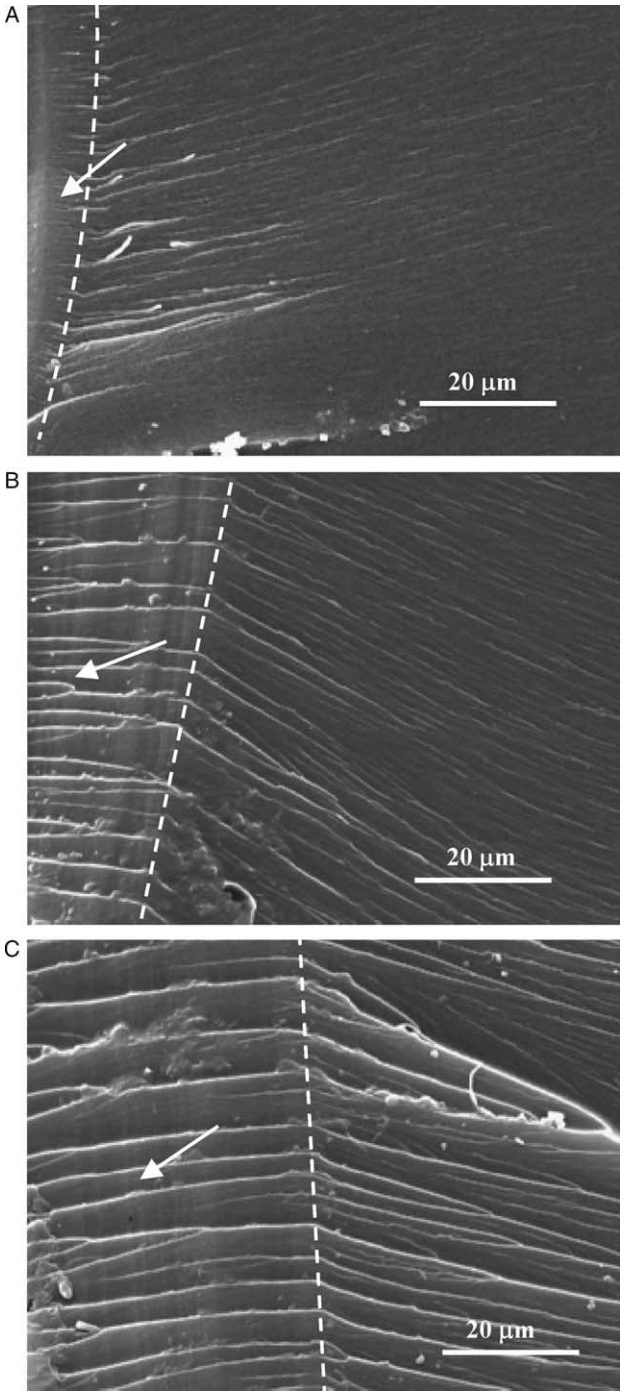

Fig. 11. SEM pictures of fractured surfaces: (A) pure epoxy resin; (B) nanocomposite with 5 wt% silica; (C) nanocomposite with 10 wt% silica. The arrow indicates the slow propagating crack area.

particles are discernible on the fractured surfaces of the specimens, even at very high magnification (40.000×), confirming the absence of aggregated particles in the nanocomposites.

In previous work based on a bis-phenol A type epoxy resin and a cycloaliphatic amine hardener [22], it was found that such a level of dispersion could not be obtained even at very low concentrations (1–2 wt% silica) unless the epoxy resin was previously functionalized with an organo-silane coupling agent. Furthermore the best dispersion was always obtained when the epoxy resin was functionalized with an amine silane coupling agent, as compared to functionalisation with either a mercaptan silane or an isocyanate silane coupling agent.

In the present study some cursory experiments with the TGDDM resin and methyl nadic anhydride hardener, also showed that dispersion of the silica could not be achieved even at low silica contents.

The micrographs of Fig. 11 show two distinct regions of crack growth: a slow propagating crack area ahead the crack tip, and a fast fracture region. Note that the crack direction is from left to right in the micrographs. It has been found in early investigations [44–46] that these features are particularly evident when a stick–slip process takes place. In fact, for the net epoxy resin, for which no stick–slip behaviour was observed, the fracture surface is quite smooth, apart from a very restrict slow crack area, which is followed by fine longitudinal lines associated with the fast crack propagation. On the other hand, for nanocomposites, where the crack propagation occurs by a stick–slip process, a well defined area of slow crack growth is evident together with V-shaped topographic features, originating from events occurring during the arrest and re-initiation of crack propagation. After this region, the crack accelerates giving rise, as in the case of the neat resin, to the formation of longitudinal lines covering the remainder of the surface.

The slow crack region is usually taken as a measure of the fracture toughness because it represents the resistance of the material against crack propagation. For the hybrid materials this region is markedly larger with respect to the plain epoxy resin and increases with increasing the silica concentration.

Since the $(K_c/\sigma_y)^2$ ratio is directly proportional to the critical crack length for the occurrence of brittle fractures, i.e. $K_c/\sigma_y = Y(a_{crit})^{1/2}$, the data in Fig. 12 reveal that the a_{crit}

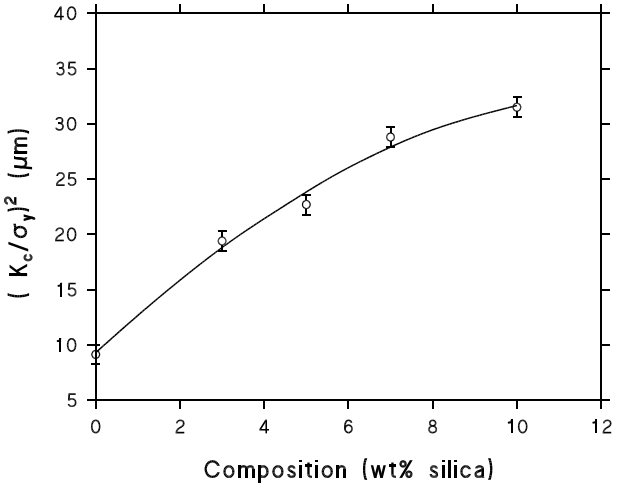

Fig. 12. $(K_c/\sigma_y)^2$ as a function of silica content.

value for the onset of brittle fracture increases with silica content up to about 10 wt%.

The resulting increase in critical crack length with increasing silica content can be considered to arise from the restrictions on segmental motions within the matrix. This makes the energy consumption for the fracture process to become more reliant on the breakage of chemical bonds than through molecular relaxations within the network.

4. Conclusions

(1) Alcohol dispersed silica-sol particles can be dispersed in TGDDM/DDS epoxy resin mixtures without forming agglomerates up to 10% w/w silica. This can be attributed to the basic character of both components of the resin mixture, which provides sufficient interactive sites for the acidic hydroxyl groups on the surface of the silica particles.
(2) FT-IR spectroscopy provided evidence of a reaction between the TGDDM epoxy groups and the silanol groups on the surface of the silica nanoparticles. This reaction contributed to enhance the interfacial strength. Neither the curing kinetics nor the final structure of the cured TGDDM/DDS epoxy resin network are affected by the presence of the silica phase.
(3) The activation volume and activation energy for yielding decrease with silica content in the opposite manner. From a linear extrapolation it is predicted that the activation volume approaches zero at around 25–30 wt% of silica, so that the segmental jump mechanism for yielding can no longer take place.
(4) The addition of silica nanoparticles up to 10 wt% brings about a considerable increase in fracture toughness and an increase in critical crack length for the onset of brittle fracture. This is responsible for the observed increase in K_c values and much larger increase in G_c values.

References

[1] Mascia L. The role of additives in plastics. London: (Edward) Arnold; 1974. p. 87–8.
[2] Davidson T. In: Xanthos M, editor. Conductive and magnetic fillers in 'functional fillers for plastics'. Weinheim, Germany: Wiley-VCH; 2005.
[3] Gatcher R, Klemchuk PR, Muller H, Andreas H. Plastics additives handbook. 4th ed. Munich: Hanser; 1993.
[4] Nakamura Y, Yamaguchi M, Okubo M, Matsumoto T. J Appl Polym Sci 1992;45:1281.
[5] Yamamoto I, Higashihara T, Kobayashi T. JSME Int J Ser, A: Solid Mech Mater Eng 2003;46:145.
[6] Nakamura Y, Yamaguchi M, Okubo M, Matsumoto T. Polymer 1991; 32:2976.
[7] Lee JY, Shim MJ, Kim SW. Polym Eng Sci 1999;39:1993.
[8] Lee J, Yee AF. J Appl Polym Sci 2001;79:1371.
[9] Wang MS, Pinnavaia TJ. Chem Mater 2004;6:468.
[10] Dean D, Walker R, Theodore MH, Nyairo E. Polymer 2005;46:3014.
[11] Ni Y, Zheng S, Nie K. Polymer 2004;45:5557.
[12] Meng J, Hu X. Polymer 2004;45:9011.
[13] Ratna D, Becker O, Krishnamurthy R, Simon GP, Varley RJ. Polymer 2003;44:7449.
[14] Kommann X, Thoman R, Mulhaupt R, Finter J, Berglund LA. Polym Eng Sci 2002;42:1815.
[15] Mascia L, Tang T. J Mater Chem 1998;8:2417.
[16] Matejeika L, Dusek K, Plestil J, Kriz J, Lednicky F. Polymer 1999;40: 171.
[17] Mascia L, Prezzi L. Adv Polym Tech 2005;24:91.
[18] Mascia L, Prezzi L, LaVormia M. Polym Eng Sci 2005;45:1039.
[19] Kinloch AJ, Lee JH, Taylor AC, Sprenger S, Eger C, Egan D. J Adhesion 2003;79:867.
[20] Liu YL, Hsu CH, Wei WL, Jeng RJ. Polymer 2003;44:5159.
[21] Schadler LS, Siegel RW. Nanostruct Mater 1999;12:507.
[22] Wetzel B, Haupert F, Friedrich K, Ming Q, Rong ZM. Polym Eng Sci 2002;42:1919.
[23] Brow F, Srawley J. ASTM Spec Tech Publ 1966;510:13.
[24] Plati E, Williams JG. Polym Eng Sci 1975;15:470.
[25] Mauritz KA, Warren RM. Macromolecules 1989;22:1730.
[26] Mondragon MA, Castano VM, Garcia J, Tellez CA. Vib Spectro 1995;9:293.
[27] Galeener FL, Lucovsky G. Phys Rev Lett 1976;37:1474.
[28] Galeener FL. Phys Rev 1979;19:4292.
[29] Musto P, Martuscelli E, Ragosta G, Russo P. High Perform Polym 2000;12:155.
[30] George GA, Cole-Clarke P, John St N, Friend G. J Appl Polym Sci 1991;42:643.
[31] Chike KE, Myrick ML, Lyon RE, Angel SM. Appl Spectrosc 1999; 10:1631.
[32] Min BG, Stachurski ZH, Hodgkin JH, Heat GR. Polymer 1993;34: 3620.
[33] De Bakker CJ, John St NA, George GA. Polymer 1993;34:716.
[34] Ragosta G, Musto P, Scarinzi G, Mascia L. Polymer 2003;44:2081.
[35] Di Liello V, Martuscelli E, Musto P, Ragosta G, Scarinzi G. J Polym Sci, Polym Phys Ed 1994;32:409.
[36] McCrum NG, Buckley CP, Bucknall CB. Principles of polymers engineering. New York: Oxford Science Publishers; 1997.
[37] Ward IM. J Mater Sci 1971;6:1397.
[38] Kinloch AJ, Show SJ, Tod DA. Hunston DL. Polymer 1983;24:1341.
[39] Sultan SN, Mc Garry F. J Polym Eng Sci 1973;13:29.
[40] Mayr AE, Cook WD, Edward GH. Polymer 1998;39:3719.
[41] Moloney AC, Kausch H, Kaiser T, Beer HR. J Mater Sci 1987;22:381.
[42] Lee J, Yee AF. Polymer 2001;42:589.
[43] Lee J, Yee AF. Polymer 2000;41:8363.
[44] Yamini S, Young RJ. J Mater Sci 1979;14:1609.
[45] Phillips DC, Scott JM, Jones MJ. Mater Sci 1978;13:311.
[46] Andrews EH. Development in polymer fracture-1. London: Applied Science; 1979.